Energy-Efficient Deep Learning via Update Sampling from a Generalized Gaussian Distribution: An Empirical Study

Anonymous authors
Paper under double-blind review

Abstract

The computation of loss gradients via backpropagation constitutes a significant portion of the energy consumption in the training of deep learning (DL) models. This paper introduces a simple yet effective method to reduce energy usage during training by leveraging the overparameterization of DL models. Under this assumption, the loss landscape is smooth, and we hypothesize that gradient elements follow a Generalized Gaussian Distribution (GGD). Based on this hypothesis, energy savings are achieved by skipping entire training epochs and estimating gradients by sampling from a GGD. Specifically, parameter updates during skipped epochs are performed by adding GGD-based samples of gradient components to the model parameters from the previous epoch. Furthermore, we present a theorem that provides an upper bound on the expected loss behavior, along with the corresponding convergence rate. We provide extensive empirical validation of our GGD hypothesis across various tasks—image classification, object detection, and image segmentation—using widely adopted DL models. Results show substantial reductions in energy consumption without compromising model performance. Additionally, we evaluate our method on Domain Adaptation (DA), Domain Generalization (DG), and Federated Learning (FL) tasks, observing similar energy savings. To further validate the adaptability of our sampling strategy, we also test it in large language model (LLM) pre-training, demonstrating its effectiveness across diverse settings.

1 Introduction

Training deep learning (DL) models is infamous for its energy consumption. This aspect has been discussed and debated due to its impact on global warming and sustainable development. The energy consumption of training and hyperparameter tuning of large DL models was studied in (Strubell et al., 2020). This work recommends AI researchers prioritise the development of energy-efficient hardware and algorithms. A more recent work discusses the energy consumption during inference (Desislavov et al., 2023) and suggests that the energy consumed for inference is growing slower than model training. However, this work also cautions that the energy requirements could escalate if the assumptions made become invalidated by increased penetration of AI-based solutions. Gradient descent-based iterative methods are employed for training DL models. Central to this training process is the forward propagation of data points to compute model predictions, followed by the back-propagation (backprop) (Rumelhart et al., 1986) of the model errors for estimating loss gradients. These gradients are used to update the model parameters. The backprop of model errors is the most energy-consuming operation during training.

In this work, we focus on reducing the number of backprop operations and improving the energy efficiency of DL model training. Also, the problem of improved energy efficiency in the federated learning (FL) framework (Li et al., 2020a) is studied using the same lens. The contributions of this work include:

- a hypothesis that the parameter update distribution is a Generalized Gaussian Distribution (GGD), and its empirical evidence,
- a simple yet effective strategy for saving energy during training based on the above hypothesis, and an extensive empirical validation of the hypothesis using popular DL models on several computer

vision tasks (like Image Classification, Object Detection, Image Segmentation, Domain Adaptation, Domain Generalization) and LLM-Pretraining,

- a stochastic version of federated learning algorithms (McMahan et al., 2017; Li et al., 2020b; Sun et al., 2023) that reduces training rounds, again based on the above hypothesis.

2 Related Work

Given the rise of foundation models Liu et al. (2023) with massive energy requirements for training, the need for energy efficiency in model training cannot be overemphasized. The design of energy-efficient methods for training DL models has received significant attention from the hardware perspective. An excellent albeit slightly dated survey of efficient processing methods for DL models is presented in Sze et al. (2017). Esser et al. (2015) proposed an approach for deploying the backprop algorithm in neuromorphic computing design. This is achieved by treating the spikes and discrete synapses as continuous probability distributions and thereby satisfying the requirement of the backprop algorithm. This approach led to significant energy savings on the TrueNorth neuromorphic architecture Merolla et al. (2014). Weight pruning is a popular algorithmic approach to efficient model training without compromising performance. Hoefler et al. (2021) present a comprehensive survey of the various techniques proposed in the literature for sparsifying DL models and Stochastic Gradient Langevin Dynamics (SGLD) Welling & Teh (2011) adds Gaussian noise sampled independently at each iteration, with a fixed zero mean and variance proportional to the step size. This noise is then directly added to the current gradient updates to ensure stochasticity and enable posterior sampling. Recent works Kuo & Madni (2022); Lin et al. (2022) propose green learning by avoiding non-linearities and the backprop algorithm altogether. Gaussian noise injection (GNI) Camuto et al. (2020) act as an explicit regulariser that suppresses high-frequency components in neural network activations, promoting smoother functions and improved generalization. MeZO Malladi et al. (2023) proposes the addition of small Gaussian noise to perturb the parameter updates. It requires only two forward passes through the model to compute the gradient estimate.

Our approach differs from existing methods by retaining backpropagation while adopting a stochastic approach to estimate gradient values, reducing the number of forward and backpropagation operations for greater energy efficiency. In contrast to SGLD Welling & Teh (2011), our method dynamically adapts injected noise based on differences in the model's parameters over time, ensuring better alignment with the parameter space and capturing training variability for improved posterior approximations and generalization. Additionally, unlike MeZO Malladi et al. (2023), our approach is versatile and can be applied to train deep learning models from scratch.

In the FL framework, a central server coordinates the training of clients by aggregating client model parameters (Li et al., 2020a). Each client updates its model parameters locally by training on its private dataset. The clients then share their model parameters with the central server. The server collates the client parameters and computes a set of global weights. These weights are then sent to the clients for use in the next training round. The two-way exchange of model parameters happens over several rounds until the models converge. Let $\boldsymbol{\theta}^{(r)}$ denote the collated parameter vector at the server, and $\boldsymbol{\theta}^{(r,k)}$ represent the client k's parameter vector after the client update at round r (using $\boldsymbol{\theta}^{(r,k)}$ as the initialization). In the FL algorithm, the server update is given by:

$$\boldsymbol{\theta}^{(r+1)} = \frac{\mathcal{D}_i}{|\mathcal{D}|} \sum_{k=1}^{K} \boldsymbol{\theta}^{(r,k)} \tag{1}$$

where K is the number of clients used, $|\mathcal{D}_k|$ is the size of data in client k and $|\mathcal{D}|$ is the size of overall dataset ($|D| = \sum_{k=1}^{K} |\mathcal{D}_k|$). We demonstrate the utility of our hypothesis in the FL framework by reducing the number of communication rounds used to train the clients.

3 Proposed Approach

3.1 Classification Setting

We operate in the classification setting with the dataset denoted by $\mathcal{D} = \{(\mathbf{x}_1, \mathbf{y}_1), (\mathbf{x}_2, \mathbf{y}_2), \ldots, (\mathbf{x}_N, \mathbf{y}_N)\}$ composed of N data points $\mathbf{x}_i \in \mathcal{X}$ and corresponding labels $\mathbf{y}_i \in \mathcal{Y}$. The data point-label pairs are assumed to be i.i.d. samples drawn from a fixed but unknown distribution $p(\mathbf{x}, \mathbf{y})$. The DL model is denoted by $f(\mathbf{x}; \boldsymbol{\theta}) : \mathcal{X} \to \mathcal{Y}$ where $\mathbf{x}$ is the input data point and the vector $\boldsymbol{\theta}$ represents the model's parameters. The loss function is defined as

$$\mathcal{L}(\boldsymbol{\theta}) = \frac{1}{n} \sum_{i=1}^{n} d(\mathbf{y}_i, f(\mathbf{x}; \boldsymbol{\theta})), \tag{2}$$

where $d(\cdot, \cdot)$ is an appropriately chosen distance function, and n is the number of training samples.

Further, assuming the standard gradient-based iterative model training approach, the parameter update expression is

$$\boldsymbol{\theta}^{(k)} = \boldsymbol{\theta}^{(k-1)} + \boldsymbol{\delta}^{(k)}, \tag{3}$$

where $\boldsymbol{\delta}^{(k)} = \mathcal{G}\left(\nabla \mathcal{L}(\boldsymbol{\theta}^{(k-1)}), h_1, h_2, \ldots, h_p\right)$ represents the parameter update at iteration k. The function $\mathcal{G}(\cdot)$ denotes an optimization rule—such as SGD, Momentum, Adam, or AdaGrad—applied to the gradient $\nabla \mathcal{L}(\boldsymbol{\theta}^{(k-1)})$ computed at $\boldsymbol{\theta}^{(k-1)}$, with hyperparameters $h_1, h_2, \ldots, h_p$.

3.2 Hypothesis

In this setting, we empirically hypothesize that at each layer ℓ

$$p(\boldsymbol{\theta}_\ell^{(k)} | \boldsymbol{\theta}_\ell^{(k-1)}) \sim \mathrm{GGD}(\mu_\ell^{(k)}, \sigma_\ell^{(k)}, \beta_\ell^{(k)}). \tag{4}$$

In other words from 3 at each layer ℓ,

$$\boldsymbol{\delta}_\ell^{(k)} = \left(\boldsymbol{\theta}_\ell^{(k)} - \boldsymbol{\theta}_\ell^{(k-1)}\right) \sim \mathrm{GGD}(\mu_\ell^{(k)}, \sigma_\ell^{(k)}, \beta_\ell^{(k)}), \tag{5}$$

where GGD denotes the Generalized Gaussian Distribution, parameterized by μ_ℓ, σ_ℓ, and β_ℓ, corresponding to the mean, scale, and shape parameters, respectively, estimated via Maximum Likelihood over $\left(\boldsymbol{\theta}^{(k)}|_\ell - \boldsymbol{\theta}^{(k-1)}|_\ell\right)$ for each layer ℓ. Specifically, the GGD is given by

$$f\left(\boldsymbol{\delta}_\ell^{(k)}; \mu^{(k)}, \sigma^{(k)}, \beta^{(k)}\right) = \frac{\beta^{(k)}}{2\sigma^{(k)}\,\Gamma\left(\frac{1}{\beta^{(k)}}\right)} \exp\left(-\left|\frac{\boldsymbol{\delta}_\ell^{(k)} - \mu^{(k)}}{\sigma^{(k)}}\right|^{\beta^{(k)}}\right), \tag{6}$$

where $\Gamma(\cdot)$ is the gamma function. We provide two supporting arguments for our hypothesis.

- From (3), we obtain:

  $$\boldsymbol{\delta}_\ell^{(k)} = \boldsymbol{\theta}_\ell^{(k)} - \boldsymbol{\theta}_\ell^{(k-1)}. \tag{7}$$

  For a mini-batch B, this becomes:

  $$\boldsymbol{\delta}_\ell^{(k)}|_B = \left(\boldsymbol{\theta}_\ell^{(k)} - \boldsymbol{\theta}_\ell^{(k-1)}\right)|_B \tag{8}$$

  where $\boldsymbol{\delta}_\ell^{(k)}|_B$ denotes the function applied to the gradient computed on mini-batch B, with respect to the model parameters $\boldsymbol{\theta}^{(k-1)}$ at layer ℓ.

  Let $\boldsymbol{\xi}_\ell^B = \boldsymbol{\delta}_\ell^{(k)}|_B - \boldsymbol{\delta}_\ell^{(k)}$ represents the stochastic noise which is the error between the mini-batch gradient and the deterministic gradient. The noise $\boldsymbol{\xi}_\ell^B$ prevents the gradient updates from becoming zero, ensuring continued exploration of the loss landscape. As optimization progresses, $\boldsymbol{\delta}_\ell^{(k)} \to 0$ near

local minima (due to the L'-Lipschitz continuity of $\mathcal{L}$), causing $\boldsymbol{\xi}_\ell^B$ to diminish. Consequently, the updates become smaller and unimodal, centered around zero.

We rewrite $\boldsymbol{\delta}_\ell^{(k)}|_B$ in (8) as:

$$\boldsymbol{\delta}_\ell^{(k)}|_B = \boldsymbol{\delta}_\ell^{(k)} + \boldsymbol{\xi}_\ell^B. \tag{9}$$

- Empirical studies by (Şimşekli et al., 2019) show that $\boldsymbol{\xi}_\ell^B$ often exhibits heavy-tailed behavior. According to the Generalized Central Limit Theorem (GCLT) (Gnedenko & Kolmogorov, 1954), the updates $\boldsymbol{\theta}_\ell^{(k)} - \boldsymbol{\theta}_\ell^{(k-1)}$ converge to a stable distribution with heavy tail.

The parameters of the GGD can be estimated using the standard maximum likelihood approach using error vector samples computed over the training epochs. In practice, however, the number of parameters in DL models is prohibitively large for efficient parameter estimation. We propose a simple workaround to overcome this practical challenge. The error vector $\boldsymbol{\delta}^{(k)}$ at the kth epoch is partitioned into layerwise i.e. $\boldsymbol{\delta}^{(k)} = \left[\boldsymbol{\delta}_1^{(k)}, \boldsymbol{\delta}_2^{(k)}, \cdots, \boldsymbol{\delta}_\ell^{(k)}, \cdots, \boldsymbol{\delta}_L^{(k)}\right]$ (assuming L layers), and modelled at the layer level. Here, $\boldsymbol{\delta}_\ell^{(k)}$ refers to the error sub-vector corresponding the ℓth layer. A further simplification is to treat all the elements of the ℓth layer error vector $\boldsymbol{\delta}_\ell^{(k)}$ as i.i.d. random variables whose distribution is given by $\text{GGD}(\mu_\ell^{(k)}, \sigma_\ell^{(k)}, \beta_\ell^{(k)})$. This can be justified by the fact that the inputs and outputs at a given layer have similar dynamic ranges due to operations such as batch normalization and layer normalization. While this may appear to be an over-simplification, it works well in practice.

3.3 Energy-Efficient Model Training

We now apply our hypothesis to achieve energy-efficient DL model training. A straightforward way is to estimate the model parameters of the layer-level GGD based on the parameter update $\boldsymbol{\delta}_\ell^{(k)}$ after some k epochs. Given that we ascribe the same GGD to all elements of $\boldsymbol{\delta}_\ell^{(k)}$, its parameters are estimated by the elements of $\boldsymbol{\delta}_\ell^{(k)}$.

During the $(k+1)^{\text{st}}$ epoch, the entire forward and backward propagations are skipped. Instead, the model update happens by sampling the parameter update from the GGD and adding these samples to the parameter $\boldsymbol{\theta}^{(k)}$. This can be expressed as:

$$\boldsymbol{\theta}_\ell^{(k+1)} = \boldsymbol{\theta}_\ell^{(k)} + \hat{\boldsymbol{\delta}}_\ell^{(k)}, \tag{10}$$

where $\hat{\boldsymbol{\delta}}_\ell^{(k)} \sim \text{GGD}(\boldsymbol{\delta}_\ell^{(k)}; \mu_\ell^{(k)}, \sigma_\ell^{(k)}, \beta_\ell^{(k)})$ samples drawn n_ℓ (size of $\boldsymbol{\delta}_\ell^{(k)}$) times from the GGD and reshaped to align with the dimensions of $\boldsymbol{\delta}_\ell^{(k)}$, ensuring uniform size and structure. The update in (10) is carried out for all L layers of the model. The proposed model training approach is summarized in Algorithm 1 we call it as **GradSamp**.

A natural question is about the frequency of using (10) for model update. Several strategies could be employed to answer this question. A simple strategy is to make this update periodic and experiment with the period. Another approach is to randomly choose an epoch and apply (10). Yet another strategy is to do sampling based upon half of the delayed epochs and apply (10). All these strategies are explored in section 4.1. We present a theorem for our sampling approach with an upper bound on the expected loss behavior $\Delta_k = \mathbb{E}[\mathcal{L}(\boldsymbol{\theta}^{(k)}) - \mathcal{L}(\boldsymbol{\theta}^{(*)})]$ along with convergence rate as follows:

Theorem 3.1 (Convergence under GGD noise)**.** *Let ρ be the sampling probability, and suppose that the update error $\boldsymbol{\theta}^{(k)}$ follows a Generalized Gaussian Distribution (GGD), with $\mathbb{E}[\boldsymbol{\theta}^{(k)}] = \mathbf{0}$ and $\mathbb{E}[\| \boldsymbol{\theta}^{(k)} \|] \leq {\sigma^{(k)}}^2$.*

Assume the loss function $\mathcal{L}(\boldsymbol{\theta})$ is μ'-strongly convex and L'-Lipschitz continuous, with optimal parameter $\boldsymbol{\theta}^{(*)}$. If the learning rate η satisfies $0 < \eta < \min\left\{\frac{2}{L'}, \frac{1}{2\mu'(1-\rho)}\right\}$, then the expected loss difference $\Delta_k = \mathbb{E}[\boldsymbol{\theta}^{(k)} - \boldsymbol{\theta}^{(*)}]$ satisfies:

$$\Delta_{k+1} \leq \gamma \Delta_k + \frac{\rho L' {\sigma^{(k)}}^2}{2},$$

where $\gamma = 1 - (1-\rho)(2\mu'\eta - L'\mu'\eta^2)$. Consequently, the convergence rate is $\mathcal{O}(\gamma^k)$.

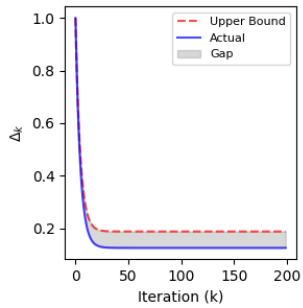

Figure 1: Convergence of Δ_K: Theoretical upper bound vs. actual values.

The detailed proof of Theorem 3.1 is provided in Section A. The plot 1 illustrates the convergence of Δ_k under the given recursive bound, where the actual values (blue line) exhibit an initial rapid decay, driven by the geometric contraction term $1-(1-\rho)(2\mu'\eta - L'\mu'\eta^2)\Delta_k$, followed by a plateau due to the additive noise-dependent term $\frac{\rho L' {\sigma^{(k)}}^2}{2}$. The theoretical upper bound (red dashed line) consistently stays above the actual values, with the shaded region representing the gap, indicating that while the bound provides a good approximation of the convergence trend,

Algorithm 1 GradSamp Algorithm

Input: Model parameters $\boldsymbol{\theta}$, training dataset $\mathcal{D} = \{(\mathbf{x}_i, \mathbf{y}_i)\}_{i=1}^n$, number of layers L, parameters per layer $\{n_\ell\}_{\ell=1}^L$, and tolerance $\varepsilon = 0.001$
Output: Trained parameters $\boldsymbol{\theta}^{(*)}$
Initialize: Epoch counter $k \leftarrow 0$
while *stopping condition not met* **do**
  if *sampling condition met* **then**
    Compute parameter update error:
    $\boldsymbol{\delta}^{(k-1)} = \boldsymbol{\theta}^{(k-1)} - \boldsymbol{\theta}^{(k-2)}$; `// From buffer`
    Partition $\boldsymbol{\delta}^{(k-1)}$ by layer:
    $\boldsymbol{\delta}^{(k-1)} = \left[\boldsymbol{\delta}_1^{(k-1)}, \boldsymbol{\delta}_2^{(k-1)}, \ldots, \boldsymbol{\delta}_L^{(k-1)}\right]$
    for $\ell \leftarrow 1$ *to* L **do**
      Fit GGD to $\boldsymbol{\delta}_\ell^{(k-1)}$:
      Obtain $\mu_\ell^{(k-1)}$, $\sigma_\ell^{(k-1)}$, and $\beta_\ell^{(k-1)}$; `// By fitting GGD to` $\boldsymbol{\delta}^{(k-1)}$
      Sample $\hat{\boldsymbol{\delta}}_\ell^{(k-1)} \sim \mathrm{GGD}(\mu_\ell^{(k-1)}, \sigma_\ell^{(k-1)} + \varepsilon, \beta_\ell^{(k-1)})$:
      Generate n_ℓ samples and reshape to match $\boldsymbol{\delta}_\ell^{(k-1)}$
      Update parameters for layer ℓ:
      $\boldsymbol{\theta}_\ell^{(k)} = \boldsymbol{\theta}_\ell^{(k-1)} + \hat{\boldsymbol{\delta}}_\ell^{(k-1)}$
    end
  end
  else
    Save $\boldsymbol{\theta}^{(k-1)}$ in buffer
    Update parameters via backpropagation:
    $\boldsymbol{\theta}^{(k)} = \boldsymbol{\theta}^{(k-1)} + \boldsymbol{\delta}^{(k)}$
  end
  $k \leftarrow k + 1$; `// Increment epoch counter`
end

Table 1: Comparison with noise-based methods.

Paper	Equation	Adaptive Noise	Skipping Epoch
SGLD (Welling & Teh, 2011)	$\boldsymbol{\theta}^{(k+1)} = \boldsymbol{\theta}^{(k)} + \frac{\epsilon_k}{2}\left(\nabla \log p(\boldsymbol{\theta}^{(k)}) + \frac{N}{n}\sum_{i=1}^{n} \nabla \log p(\mathbf{x}_i \mid \boldsymbol{\theta}^{(k)})\right) + \eta_k;\ \eta_k \sim \mathcal{N}(0, \epsilon_k I)$	✗	✗
GNI (Camuto et al., 2020)	$\tilde{h}_k(x) = \hat{h}_k(x) + \epsilon_k;\ \epsilon_k \sim \mathcal{N}(0, \sigma_k^2 I)$	✗	✗
MeZO (Malladi et al., 2023)	$\boldsymbol{\theta}^{(k+1)} = \boldsymbol{\theta}^{(k)} + \frac{\mathcal{L}(\boldsymbol{\theta}^{(k)}+\epsilon z;\mathcal{B}) - \mathcal{L}(\boldsymbol{\theta}^{(k)}-\epsilon z;\mathcal{B})}{2\epsilon} z; \quad z \sim \mathcal{N}(0, I)$	✗	✗
Ours	$\boldsymbol{\theta}_\ell^{(k+1)} = \boldsymbol{\theta}_\ell^{(k)} + \hat{\boldsymbol{\delta}}_\ell^{(k)}; \quad \hat{\boldsymbol{\delta}}_\ell^{(k)} \sim \mathrm{GGD}((\boldsymbol{\theta}_\ell^{(k-1)} - \boldsymbol{\theta}_\ell^{(k)}); \mu_\ell^{(k)}, \sigma_\ell^{(k)}, \beta_\ell^{(k)})$	✓	✓

3.4 Comparison with other noise-based strategies

As shown in Table 1, unlike SGLD (Welling & Teh, 2011), our method does not inject fixed Gaussian noise at each iteration for posterior sampling $p(\mathbf{x} \mid \boldsymbol{\theta}^{(k)})$, nor does it resemble Gaussian noise injection (GNI) (Camuto et al., 2020), which perturbs the activation space $\hat{\boldsymbol{h}}(\mathbf{x})$ to regularize the model. Unlike MeZO (Malladi et al., 2023), which estimates gradients using symmetric perturbations via two forward passes (over batch size B with some perturbation scale ϵ), our approach adaptively estimates parameter updates using temporal differences in the parameter trajectory. Furthermore, existing methods primarily focus on improving model performance without addressing the cost of backpropagation. In contrast, our method explicitly aims to skip backpropagation steps, achieving energy efficiency without compromising model accuracy.

3.5 Stochastic Federated Learning Algorithms

We found the FL framework to be a natural fit to test our hypothesis in a distributed learning setting. Specifically, we claim that the elements of $\boldsymbol{\delta}^{(r)} = \boldsymbol{\theta}^{(r)} - \boldsymbol{\theta}^{(r-1)}$ follow a unimodal GGD (using the notation from (1) and r being the round index). In other words,

$$p(\boldsymbol{\theta}_\ell^{(r)} | \boldsymbol{\theta}_\ell^{(r-1)}) \sim \mathrm{GGD}(\mu_\ell^{(r)}, \sigma_\ell^{(r)}, \beta_\ell^{(r)}) \tag{11}$$

We modify We modify the `FedAvg` (McMahan et al., 2017), `FedProx` (Li et al., 2020b) and `FedSpeed` (Sun et al., 2023) algorithms to their stochastic variants where the update rule becomes:

$$\boldsymbol{\theta}_\ell^{(r+1)} = \boldsymbol{\theta}_\ell^{(r)} + \hat{\boldsymbol{\delta}}_\ell^{(r)} \tag{12}$$

where $\hat{\boldsymbol{\delta}}_\ell^{(r)} \sim \mathrm{GGD}(\boldsymbol{\delta}_\ell^{(r)}; \mu_\ell^{(r)}, \sigma_\ell^{(r)}, \beta_\ell^{(r)})$ samples drawn n_ℓ (size of $\boldsymbol{\delta}_\ell^{(r)}$) times from the GGD and reshaped to align with the dimensions of $\boldsymbol{\delta}_\ell^{(r)}$, ensuring uniform size and structure.

4 Experiments and Results

The proposed hypothesis and energy-based model are empirically validated across a wide range of computer vision tasks, including image classification, object detection, image segmentation, Domain Adaptation (DA), Domain Generalization (DG), and Federated Learning (FL) under both IID and Non-IID settings. Additionally, the method is evaluated on Large Language Model (LLM) training to demonstrate its broader applicability. More technical and implementation details were found in the sections B and C of the supplementary material.

4.1 Sampling Strategies

We explored four strategies to trigger the energy-saving mechanism. For periodic sampling (Pe), we used intervals of 5 and 10 epochs. Probabilistic (Pr) sampling drew from a `Bernoulli(`ρ`)` distribution with $\rho = 0.2, 0.5$, and 0.7, sampling gradients whenever a 1 was drawn. In Delayed Period (DP) sampling, no sampling occurred during the first half of the epochs, followed by periodic sampling with intervals of 5 and 10. Similarly, Delayed Random (DR) sampling skipped the first half of the epochs, then applied random sampling with probabilities $\rho = 0.2, 0.5$, and 0.7.

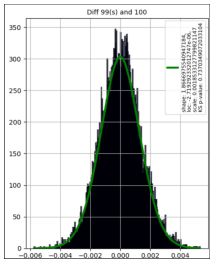

Scale: 1.853×10^{-3}
Loc: -2.793×10^{-6}
Shape: 1.867
KS p-value: 0.773

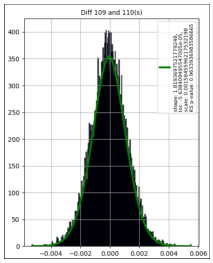

Scale: 1.585×10^{-3}
Loc: -5.638×10^{-5}
Shape: 1.819
KS p-value: 0.963

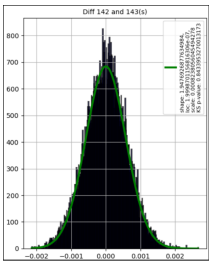

Scale: 8.204×10^{-4}
Loc: 2.000×10^{-7}
Shape: 1.948
KS p-value: 0.843

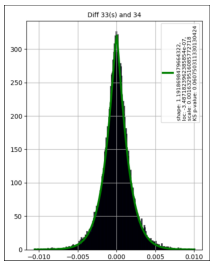

Scale: 1.633×10^{-3}
Loc: 4.872×10^{-7}
Shape: 1.192
KS p-value: 0.061

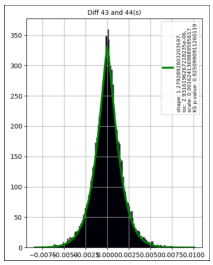

Scale: 1.624×10^{-3}
Loc: 3.162×10^{-6}
Shape: 1.173
KS p-value: 0.925

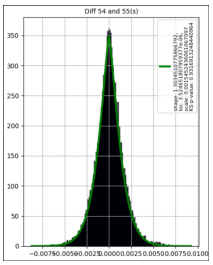

Scale: 1.545×10^{-3}
Loc: 5.247×10^{-6}
Shape: 1.303
KS p-value: 0.932

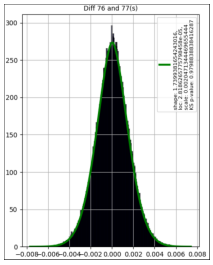

Scale: 2.047×10^{-3}
Loc: 2.819×10^{-5}
Shape: 1.740
KS p-value: 0.980

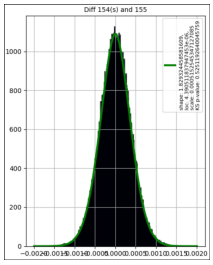

Scale: 5.153×10^{-4}
Loc: 4.391×10^{-6}
Shape: 1.829
KS p-value: 0.525

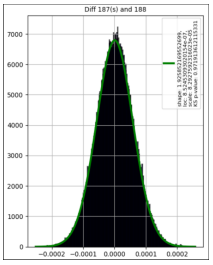

Scale: 8.293×10^{-5}
Loc: 8.525×10^{-7}
Shape: 1.926
KS p-value: 0.972

Figure 2: Parameter update histograms (fitted with GGD) across three architectures on the Tiny-ImageNet dataset, sampled every 10 epochs. **Top row:** ResNet-50 at the 1st convolution, 2nd stage, and 2nd residual block (Epochs 100, 110, 143). **Middle row:** Swin-T QKV weights at the 1st layer and 2nd block (Epochs 33, 44, 55). **Bottom row:** MLP-Mixer at the 3rd layer, 2nd stage, and 1st fully connected layer (Epochs 77, 155, 188).

4.2 Results

Image Classification: For the image classification task, we experimented with various baseline networks (He et al., 2016; Liu et al., 2021; Tolstikhin et al., 2021). Qualitative results, shown in the sub-plots present in 2, provide empirical support for our hypothesis. The parameter update histogram at different instances confirm that our hypothesis holds across CNN, Transformer, and Non-CNN/Non-Transformer networks. The standard Kolmogorov-Smirnov (KS)-test (Massey, 1951) goodness of fit with a probability value $p = 5\%$. Upon clear examination of these plots, the mean (loc) and standard deviation (scale) values are approximately zero, and the values of shape parameters are less than 2. This clearly indicates that the parameter updates

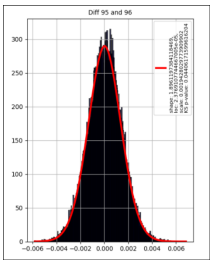

Scale: 1.943×10^{-3}
Loc: 2.377×10^{-5}
Shape: 1.896
KS p-value: 0.044

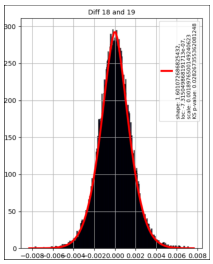

Scale: 1.898×10^{-3}
Loc: -7.315×10^{-7}
Shape: 1.601
KS p-value: 0.028

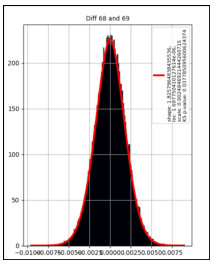

Scale: 2.485×10^{-3}
Loc: 1.698×10^{-6}
Shape: 1.826
KS p-value: 0.038

Figure 3: Failure cases in parameter update histograms (fitted with GGD) across different architectures on the Tiny-ImageNet dataset, sampled every 10 epochs. **Left:** ResNet-50 (2nd Conv, 2nd Stage, 2nd Residual Block, epoch 96). **Middle:** Swin-T (2nd Conv, 2nd Stage, 2nd Layer, epoch 19). **Right:** MLP-Mixer (1st FC Layer, 2nd Stage, 3rd Layer, epoch 96).

are heavy-tailed and fit a nice GGD envelope (in green color). However, even in the failure cases present in figure 3, the parameter update histogram followed a unimodal behavior centered at zero with nearly zero standard deviation, and were fitted by a skewed GGD envelope (in red color). Additionally, it is worth noting that the hypothesis holds better as the number of training epochs increases. Furthermore, the qualitative results reveal that the GGD hypothesis is valid in the convolution layers of CNNs, QKV parameters in transformer models and FC layers in mixer models. This observation aligns with the larger number of parameters present in these layers compared to others.

By examining Table 2, we can estimate energy savings based on the skipped backpropagation operations, as backpropagation accounts for a significant portion of training energy consumption. The proposed approaches are compared against the baseline performance, which is presented in the first row for each model. A key observation is that simple periodic sampling with periods of 5 and 10 epochs leads to energy savings without a significant performance drop across all models, including standard deep learning models, transformer-based architectures, and mixer models. Similarly, the random sampling strategy, where backpropagation is replaced with Generalized Gaussian Distribution (GGD) samples 20% of the time, shows no notable performance degradation. In other words, the proposed method achieves nearly identical model performance while reducing energy consumption by up to 20% compared to the baseline. Given the large scale at which deep learning models are trained, this represents a substantial energy-saving opportunity and highlights the effectiveness of a simple periodic sampling approach. However, a noticeable performance drop is observed when sampling frequencies increase. Importantly, this degradation remains consistent as energy savings increase from 20% to 70%. A similar trend is observed in delayed sampling approaches such as DP and DR, which result in approximately 5% and 20% energy savings, respectively.

Impact on ImageNet (Deng et al., 2009): The results in Table 3 demonstrate that incorporating our sampling strategies can significantly reduce computational cost on the ImageNet dataset without compromising model performance. In particular, probabilistic sampling with a probability of 0.2 consistently outperforms the baseline in top-5 and top-10 accuracy across all architectures—ResNet-50, Swin-T, and MLP-Mixer—while achieving up to 20% computational savings. Similarly, periodic sampling with an interval of 10 yields competitive results with minimal accuracy drop and only 10% resource usage reduction. This highlights the effectiveness of using parameter update histogram-guided sampling over GGD-based energy distributions to selectively trigger updates, allowing for better energy-efficiency and scalability in large-scale vision tasks like ImageNet classification.

Object Detection: In the object detection setting, we evaluated our sampling strategies using real-time object detectors such as YOLOv7 (Wang et al., 2023) and RT-DETRv2 (Lv et al., 2024), as shown in table 4.

Table 2: Performance comparison of standard models under diverse sampling strategies, including periodic (Pe), probabilistic (Pr), delayed periodic (DP), and delayed random (DR) samplings, along with total FLOPS (in Tera FLOPS (TFLOPS)) over 200 epochs for 3 independent trials. Best values are **bolded**.

Model	Strategy (% savings)	CIFAR-10		Total TFLOPS	CIFAR-100		Total TFLOPS	TINY		Total TFLOPS
		Acc @1(↑)	*Acc* @5(↑)		*Acc* @1(↑)	*Acc* @5(↑)		*Acc* @1(↑)	*Acc* @5(↑)	
ResNet-50	Baseline (0)	91.55 ± 0.01	99.76 ± 0.01	246716.268	69.96 ± 0.56	91.64 ± 0.25	246738.386	66.38 ± 0.96	86.22 ± 1.05	493525.924
	Pe = 5 (20)	90.87 ± 0.25	99.71 ± 0.06	206008.083	68.02 ± 0.86	90.39 ± 0.20	206026.552	64.90 ± 0.71	85.39 ± 0.30	412094.146
	Pe = 10 (10)	**91.66 ± 0.18**	**99.86 ± 0.04**	225745.385	**69.98 ± 0.33**	**91.86 ± 0.04**	225765.623	**66.40 ± 0.85**	**86.89 ± 0.16**	451576.22
	Pr = 0.2 (20)	**91.93 ± 0.08**	**99.79 ± 0.06**	217110.315	68.42 ± 1.34	**91.77 ± 0.42**	217129.78	**66.89 ± 1.37**	**86.70 ± 0.76**	434302.813
	Pr = 0.5 (50)	89.94 ± 0.31	99.69 ± 0.01	166533.481	65.90 ± 1.36	89.71 ± 0.49	166548.41	61.59 ± 1.67	83.82 ± 1.44	333129.999
	Pr = 0.7 (70)	89.28 ± 0.06	99.59 ± 0.03	146796.179	64.21 ± 1.07	89.05 ± 0.29	146809.34	60.64 ± 1.06	83.11 ± 1.37	293647.925
	DP = 5 (10)	91.32 ± 0.23	99.75 ± 0.05	234380.454	69.53 ± 0.64	90.90 ± 0.21	234401.467	65.20 ± 0.28	86.22 ± 0.06	468849.628
	DP = 10 (5)	**91.61 ± 0.08**	**99.78 ± 0.02**	240548.361	**69.98 ± 0.25**	**91.70 ± 0.20**	240569.926	**66.63 ± 0.47**	**86.27 ± 0.33**	481187.776
	DR = 0.2 (10)	91.23 ± 0.21	**99.8 ± 0.03**	234380.454	**70.06 ± 0.04**	**91.73 ± 0.05**	234401.467	**66.39 ± 0.11**	**86.39 ± 0.38**	468849.628
	DR = 0.5 (25)	90.86 ± 0.33	99.69 ± 0.03	215876.734	68.18 ± 0.00	90.81 ± 0.01	215896.088	64.82 ± 0.40	85.52 ± 0.48	431835.183
	DR = 0.7 (35)	91.06 ± 0.06	99.70 ± 0.02	203540.921	68.27 ± 0.14	90.73 ± 0.04	203559.168	64.14 ± 0.25	85.77 ± 0.18	407158.887
Swin-T	Baseline (0)	86.27 ± 1.05	99.33 ± 0.18	261786.175	64.53 ± 1.54	88.58 ± 1.92	261790.322	62.74 ± 1.18	84.69 ± 1.14	523589.861
	Pe = 5 (20)	84.39 ± 1.11	99.22 ± 0.11	218591.456	61.95 ± 1.83	87.05 ± 1.44	218594.919	60.80 ± 1.98	83.28 ± 1.48	437197.534
	Pe = 10 (10)	**86.36 ± 1.41**	**99.36 ± 0.12**	239534.35	**64.86 ± 1.54**	**88.66 ± 1.05**	239538.145	**62.75 ± 1.16**	**84.99 ± 1.15**	479084.723
	Pr = 0.2 (20)	**86.81 ± 1.67**	**99.35 ± 0.15**	230371.834	**64.58 ± 1.01**	**88.59 ± 1.62**	230375.484	**62.83 ± 1.22**	**84.99 ± 1.48**	460759.078
	Pr = 0.5 (50)	82.17 ± 1.18	98.97 ± 0.24	176705.668	57.99 ± 1.76	84.96 ± 1.64	176708.468	58.53 ± 1.59	81.63 ± 1.71	353423.156
	Pr = 0.7 (70)	80.45 ± 1.73	98.95 ± 0.06	155762.774	55.41 ± 1.03	83.25 ± 4.05	155765.242	57.58 ± 1.63	80.94 ± 1.81	311535.967
	DP = 5 (10)	84.61 ± 0.50	99.20 ± 0.09	248696.866	61.13 ± 0.37	86.72 ± 0.23	248700.806	61.62 ± 0.31	83.82 ± 0.17	497410.368
	DP = 10 (5)	**86.92 ± 0.27**	**99.37 ± 0.12**	255241.521	**64.57 ± 0.19**	**88.96 ± 0.16**	255245.564	**62.75 ± 0.06**	**85 ± 0.07**	510500.114
	DR = 0.2 (10)	**86.56 ± 0.57**	**99.38 ± 0.02**	248696.866	**64.99 ± 0.06**	**88.78 ± 0.36**	248700.806	**62.77 ± 0.49**	**84.99 ± 0.44**	497410.368
	DR = 0.5 (25)	83.96 ± 0.03	99.12 ± 0.08	229062.903	60.39 ± 0.22	85.95 ± 0.28	229066.532	61.19 ± 0.27	83.79 ± 0.04	458141.128
	DR = 0.7 (35)	83.63 ± 0.29	99.13 ± 0.06	215973.595	59.60 ± 0.04	85.82 ± 0.25	215977.016	60.59 ± 0.16	83.37 ± 0.38	431961.635
MLP-Mixer	Baseline (0)	81.99 ± 1.32	98.95 ± 0.23	155631.206	58.04 ± 1.43	83.71 ± 1.44	155633.971	54.02 ± 1.59	77.88 ± 1.35	311274.086
	Pe = 5 (20)	80.61 ± 1.21	98.93 ± 0.11	129952.057	55.23 ± 0.92	82.11 ± 0.91	129954.366	51.71 ± 1.31	76.22 ± 1.43	259913.862
	Pe = 10 (10)	**82.20 ± 0.83**	**98.96 ± 0.15**	142402.554	**58.31 ± 1.36**	**83.80 ± 1.05**	142405.084	**54.85 ± 1.50**	**77.85 ± 1.39**	284815.789
	Pr = 0.2 (20)	**82 ± 1.44**	**98.99 ± 0.13**	136955.462	**58.20 ± 1.04**	**83.73 ± 1.20**	136957.895	**54.65 ± 1.43**	77.86 ± 1.49	273921.196
	Pr = 0.5 (50)	78.96 ± 1.29	98.66 ± 0.25	105051.064	52.71 ± 1.92	80.73 ± 1.39	105052.931	48.97 ± 1.43	73.96 ± 1.22	210110.008
	Pr = 0.7 (70)	77.31 ± 1.36	98.55 ± 0.21	92600.568	50.76 ± 1.17	79.54 ± 0.76	92602.213	46.52 ± 1.48	72.66 ± 1.33	185208.081
	DP = 5 (10)	80.49 ± 1.21	98.82 ± 0.03	147849.646	56.09 ± 0.42	82.68 ± 0.04	147852.273	51.99 ± 1.50	76.36 ± 1.44	295710.382
	DP = 10 (5)	**82.05 ± 0.93**	**98.97 ± 0.04**	151740.426	**58.36 ± 0.57**	**83.73 ± 0.17**	151743.122	**54.96 ± 1.50**	77.86 ± 1.28	303492.234
	DR = 0.2 (10)	81.22 ± 0.85	**98.96 ± 0.07**	147849.646	**58.14 ± 0.57**	**83.75 ± 0.04**	147852.273	**54.87 ± 1.43**	**77.89 ± 1.26**	295710.382
	DR = 0.5 (25)	80.27 ± 1.13	98.78 ± 0.06	136177.306	55.24 ± 0.28	82.34 ± 0.00	147852.273	51.00 ± 1.37	75.94 ± 1.22	272364.826
	DR = 0.7 (35)	80.00 ± 1.18	98.79 ± 0.03	128395.745	55.08 ± 0.76	82.10 ± 0.12	128398.026	50.78 ± 1.49	75.68 ± 1.35	256801.121

Table 3: Performance comparison of standard models upon ImageNet dataset under diverse sampling strategies, including periodic (Pe), probabilistic (Pr) samplings over 100 epochs for 3 independent trials. Best values are **bolded**.

Strategy (% savings)	ResNet-50		Swin-T		MLP-Mixer	
	Acc @1(↑)	*Acc* @5(↑)	*Acc* @1(↑)	*Acc* @5(↑)	*Acc* @1(↑)	*Acc* @5(↑)
Baseline (0)	57.75±1.23	77.25±0.89	55.45±1.05	75.15±0.98	47.32±1.40	65.45±0.95
Pe = 5 (20)	56.85±0.94	77.15±1.67	55.25±0.79	74.95±1.53	45.75±0.85	64.25±1.42
Pe = 10 (10)	**57.82±1.45**	**78.65±0.76**	**55.47±1.31**	**76.75±1.08**	**48.07±1.67**	**65.75±0.83**
Pr = 0.2 (20)	**58.05±0.92**	**78.20±1.31**	**56.07±1.45**	**76.20±0.72**	**48.01±1.15**	**65.65±1.31**
Pr = 0.5 (50)	55.08±1.56	76.65±0.84	54.38±0.91	74.65±1.60	45.25±0.78	63.25±1.49
Pr = 0.7 (70)	56.00±0.74	76.85±1.42	53.07±1.22	73.85±1.35	46.09±1.53	63.75±0.92

By examining the results from the table, RT-DETRv2 (Lv et al., 2024) consistently outperforms the Baseline in both mAP @.5 and mAP @.5 : .95 for all sampling strategies, except at Pr = 0.2 for mAP @.5, where it matches the Baseline. For YOLOv7 (Wang et al., 2023), sampling strategies Pe = 10 and Pr = 0.2 demonstrate better performance than the Baseline while achieving energy reductions of 10% and 20%, respectively. These reductions result from skipping epochs, thereby lowering the total effective TFLOPS.

Image Segmentation: For the image segmentation task, we evaluated the performance of the widely used U-Net (Ronneberger et al., 2015) and the transformer-based Segmenter (Strudel et al., 2021) models,

Table 4: Performance comparison of various sampling strategies on detection models, **YOLOv7** and **RT-DETRv2**, evaluated on the PascalVOC-2012 dataset over 3 independent trials. Best results are highlighted in **bold**.

Strategy (% savings)	YOLOv7		RT-DETRv2	
	mAP @.5 (↑)	*mAP* @.5 : .95 (↑)	*mAP* @.5 (↑)	*mAP* @.5 : .95 (↑)
Baseline (0)	77.1 ± 0.73	59.6 ± 1.22	81.6 ± 1.35	66.7 ± 0.88
Pe = 5 (20)	76.0 ± 1.03	58.5 ± 0.84	**81.9 ± 1.15**	**67.1 ± 0.72**
Pe = 10 (10)	**77.4 ± 0.95**	**59.7 ± 1.04**	**82.0 ± 1.19**	**67.4 ± 0.81**
Pr = 0.2 (20)	**77.2 ± 0.82**	**59.9 ± 0.93**	81.6 ± 1.21	**66.9 ± 0.94**
Pr = 0.5 (50)	75.9 ± 1.04	58.2 ± 0.52	**82.0 ± 0.84**	**67.1 ± 0.92**
Pr = 0.7 (70)	74.8 ± 0.75	57.1 ± 1.02	**82.2 ± 1.07**	**67.1 ± 0.64**

Table 5: Performance comparison of different sampling strategies on segmentation models, **U-Net** and **Segmenter**, evaluated on the ADE20K dataset over 3 independent trials. Best results are highlighted in **bold**.

Strategy (% savings)	U-Net		Segmenter	
	SS-IoU (↑)	*MS-IoU* (↑)	*SS-IoU* (↑)	*MS-IoU* (↑)
Baseline (0)	27.50 ± 1.34	28.42 ± 1.15	38.02 ± 1.52	38.78 ± 1.23
Pe = 5 (20)	26.53 ± 1.73	27.31 ± 1.65	37.94 ± 1.14	**38.84 ± 0.98**
Pe = 10 (10)	**27.53 ± 1.91**	**28.52 ± 1.04**	**38.15 ± 1.46**	**38.91 ± 1.32**
Pr = 0.2 (20)	**27.75 ± 1.54**	**28.50 ± 1.27**	**38.16 ± 0.83**	**38.79 ± 1.64**
Pr = 0.5 (50)	25.13 ± 0.91	25.73 ± 1.42	36.26 ± 0.78	38.24 ± 1.12
Pr = 0.7 (70)	23.91 ± 0.67	24.49 ± 0.84	36.16 ± 1.05	37.37 ± 1.82

as presented in Table 5. The results demonstrate that sampling strategies such as Pe = 10 and Pr = 0.2 consistently outperform the baseline in terms of both *SS-IoU* and *MS-IoU*. These strategies enable significant energy savings of 10% and 20%, respectively. The observed reduction in energy consumption is primarily attributed to the skipped epochs during training, which directly decrease the effective TFLOPS required. This finding highlights the potential of incorporating such sampling strategies to balance model performance with computational efficiency, making them particularly beneficial in resource-constrained scenarios.

Domain Adaptation (DA) and Domain Generalization (DG): Domain Adaptation (DA) focuses on transferring knowledge from a labeled source domain to an unlabeled target domain, addressing distribution shifts. Domain Generalization (DG), on the other hand, aims to learn models that perform well on unseen target domains without accessing their data during training. We experimented with some of DA strategies like Marginal Disparity Descrepency (MDD) and Minimum Class Confusion (MCC) upon Office-31 (Saenko et al., 2010) dataset. While for DG we experimentedd with VREx (Krueger et al., 2021) and GroupDRO (Sagawa et al., 2020) upon PACS (Li et al., 2017) as shown in the tables 6 and 7

Table 6: Performance comparision of different sampling strategies on DA methods, **MDD** and **MCC**, evaluated upon Office-31 dataset over 3 independent trials. Best results are highlighted in **bold**.

Method	Strategy (% savings)	A-W	D-W	W-D	A-D	D-A	W-A
MDD	Baseline (0)	92.15 ± 0.89	98.53 ± 0.07	99.93 ± 0.12	91.96 ± 0.88	74.81 ± 0.87	72.25 ± 1.15
	Pe = 5 (20)	**92.91 ± 0.14**	**98.57 ± 0.19**	**100.00 ± 0.00**	**92.03 ± 1.21**	**74.94 ± 0.84**	71.95 ± 0.87
	Pe = 10 (10)	**92.74 ± 0.88**	98.49 ± 0.13	99.93 ± 0.12	**93.37 ± 0.60**	**74.84 ± 0.95**	**72.44 ± 0.87**
	Pr = 0.2 (20)	91.65 ± 0.85	98.53 ± 0.19	99.93 ± 0.12	**92.63 ± 1.31**	**74.90 ± 0.88**	**72.39 ± 0.35**
	Pr = 0.5 (50)	91.99 ± 1.58	**98.78 ± 0.19**	**100.00 ± 0.00**	**92.83 ± 1.82**	73.68 ± 0.84	71.47 ± 0.06
	Pr = 0.7 (70)	91.15 ± 0.19	**98.90 ± 0.19**	**100.00 ± 0.00**	91.83 ± 0.65	73.42 ± 1.15	71.00 ± 1.67
MCC	Baseline (0)	93.29 ± 0.19	98.27 ± 0.08	99.72 ± 0.12	93.64 ± 0.46	75.24 ± 0.86	74.54 ± 0.94
	Pe = 5 (20)	**93.38 ± 0.28**	98.15 ± 0.14	99.72 ± 0.12	**93.84 ± 0.64**	**75.49 ± 0.73**	74.52 ± 0.82
	Pe = 10 (10)	93.24 ± 0.36	**98.36 ± 0.08**	99.66 ± 0.12	**93.67 ± 1.06**	**75.37 ± 0.37**	**74.57 ± 0.62**
	Pr = 0.2 (20)	**93.50 ± 0.14**	**98.53 ± 0.13**	99.72 ± 0.12	**94.17 ± 0.40**	**75.52 ± 0.62**	**74.6 ± 0.85**
	Pr = 0.5 (50)	93.24 ± 0.08	**98.31 ± 0.07**	99.72 ± 0.12	93.57 ± 0.53	**75.26 ± 0.56**	74.37 ± 0.80
	Pr = 0.7 (70)	**93.55 ± 0.33**	98.27 ± 0.08	99.72 ± 0.12	**93.73 ± 1.29**	**75.27 ± 0.38**	**74.58 ± 0.48**

Table 7: Performance comparision of different sampling strategies on DG methods, **Vrex** and **GroupDRO**, evaluated upon PACS dataset over 3 independent trials. Best results are highlighted in **bold**.

Method	Strategy (% savings)	P	A	C	S
Vrex	Baseline (0)	97.66 ± 0.18	87.84 ± 0.69	79.45 ± 1.08	80.72 ± 2.05
	Pe = 5 (20)	97.44 ± 0.38	**88.36 ± 1.93**	79.19 ± 0.28	80.39 ± 0.62
	Pe = 10 (10)	**97.76 ± 0.09**	**88.34 ± 0.59**	**80.90 ± 1.71**	**81.65 ± 1.11**
	Pr = 0.2 (20)	**97.76 ± 0.28**	87.71 ± 1.88	**80.23 ± 1.52**	**81.89 ± 0.38**
	Pr = 0.5 (50)	97.52 ± 0.28	**87.98 ± 0.32**	**80.69 ± 0.39**	**81.38 ± 2.51**
	Pr = 0.7 (70)	97.05 ± 0.27	**88.34 ± 1.25**	**80.02 ± 2.15**	**81.82 ± 2.12**
GroupDRO	Baseline (0)	97.92 ± 0.15	88.60 ± 0.23	80.46 ± 1.90	79.32 ± 2.32
	Pe = 5 (20)	97.70 ± 0.03	**88.96 ± 1.01**	**81.05 ± 0.39**	**79.74 ± 2.59**
	Pe = 10 (10)	**97.98 ± 0.33**	**88.98 ± 0.16**	**80.96 ± 1.86**	**79.36 ± 1.58**
	Pr = 0.2 (20)	**97.99 ± 0.27**	**88.99 ± 0.93**	**80.90 ± 1.33**	**79.90 ± 0.28**
	Pr = 0.5 (50)	97.66 ± 0.16	88.42 ± 1.14	80.09 ± 1.59	78.95 ± 0.96
	Pr = 0.7 (70)	97.50 ± 0.33	**88.99 ± 1.74**	79.96 ± 1.75	78.90 ± 1.77

From the results in tables 6 and 7, it is evident that most of the sampling strategies for **MDD** (Zhang et al., 2019), **MCC** (Jin et al., 2020), **Vrex** (Krueger et al., 2021), and **GroupDRO** (Sagawa et al., 2020) outperform the Baseline models. In particular, the strategies with Pe = 10 and Pr = 0.2 stand out, yielding substantial improvements that result in energy savings of up to 10% and 20%. This underscores the effectiveness of our sampling strategy in promoting energy efficiency, even in the context of domain shifts, where models must adapt to an unknown target domain.

Federated Learning (FL): We evaluated the FL agorithms (McMahan et al., 2017; Li et al., 2020b; Sun et al., 2023) upon different sampling strategies and summarized in table 8 for both IID and Non-IID cases. For the Non-IID split, we use the `Dirichlet` distribution (Hsu et al., 2019) with a parameter of 0.6. Upon

Table 8: Performance comparision of differrent sampling strategies upon FL methods like `FedAvg`, `FedProx` and `FedSpeed`, evaluated upon CIFAR-10 dataset over 3 independent trails. Best results are highlighted in **bold.**

Strategy (% savings)	`FedAvg`		`FedProx`		`FedSpeed`	
	IID	*Non-IID (Dir 0.6)*	*IID*	*Non-IID (Dir 0.6)*	*IID*	*Non-IID (Dir 0.6)*
Baseline (0)	82.62 ± 1.05	80.80 ± 0.97	79.40 ± 1.34	77.51 ± 1.42	87.47 ± 0.82	86.52 ± 0.94
Pe = 5 (20)	82.35 ± 1.13	**80.82 ± 1.02**	**79.54 ± 0.89**	**78.18 ± 1.01**	87.43 ± 1.10	86.01 ± 0.78
Pe = 10 (10)	**82.71 ± 0.91**	**81.01 ± 1.34**	**79.55 ± 1.26**	**77.85 ± 1.10**	**87.53 ± 0.88**	**86.58 ± 1.33**
Pr = 0.2 (20)	**82.72 ± 0.88**	**80.91 ± 1.26**	**79.51 ± 1.03**	77.44 ± 0.98	**87.49 ± 1.29**	**86.56 ± 1.16**
Pr = 0.5 (50)	81.81 ± 1.14	79.67 ± 0.93	79.20 ± 0.94	**77.79 ± 1.16**	85.79 ± 0.77	85.79 ± 1.48
Pr = 0.7 (70)	81.75 ± 0.76	80.08 ± 1.27	79.34 ± 1.05	**77.97 ± 1.37**	85.04 ± 1.12	85.04 ± 0.96

inspecting Table 8, most federated learning (FL) algorithms outperform the baseline, with Pe = 10 and Pr = 0.2 achieving 10% and 20% energy savings, respectively. These gains are particularly valuable in FL, where multiple local epochs reduce energy consumption and FLOPs, enhancing computational efficiency.

Thus, strategies like Pe = 10 and Pr = 0.2 strike a balance between performance, energy savings, and efficiency, improving scalability and practicality for resource-constrained, real-world FL applications.

LLM Pre-training: We evaluated our sampling strategies on GPT-2 (Radford et al., 2019) fine-tuned over the IMDB dataset (Maas et al., 2011) for 20 epochs using the Adam optimizer (learning rate = 0.02). The results 9 demonstrate consistent improvements across multiple metrics. Importantly, these improvements are achieved alongside substantial energy savings—up to 70% in some cases—demonstrating the practicality of our sampling strategy for efficient training of large language models, where computational cost is a critical concern.

Optimizers: We tested our sampling approaches on various optimizers, including AdaGrad (Duchi et al., 2011) and AdaDelta (Zeiler, 2012), to assess their impact on energy savings. A careful analysis of the results in Table 10 demonstrates that our sampling methods can be successfully applied to different optimizers

Table 9: Performance comparison of different sampling strategies applied to GPT-2 (Radford et al., 2019) fine-tuned on the IMDB (Maas et al., 2011) dataset, evaluated over 3 independent trials. Best results are highlighted in **bold**.

Strategy (% savings)	**Accuracy** (↑)	**Precision** (↑)	**Recall** (↑)	**F1-score** (↑)	**Avg**
Baseline (0)	55.74	92.96	12.65	22.27	45.91
Pe=5 (20)	55.68	87.56	**13.49**	**23.37**	45.53
Pe=10 (10)	**55.88**	**93.12**	**13.05**	**22.95**	**46.25**
Pr=0.2 (20)	**56.02**	92.75	**13.20**	**23.10**	**46.27**
Pr=0.5 (50)	**56.14**	89.22	**14.21**	**24.51**	**46.02**
Pr=0.7 (70)	**55.86**	89.03	**13.61**	**23.61**	45.53

without sacrificing performance. Notably, in the cases of Pe = 10 and Pr = 0.2, the energy savings achieved were 10% and 20%, respectively.

Table 10: Impact of Different Optimizers (Ada-Grad vs. Ada-Delta) on Accuracy (%). Mean ± Std are reported for each strategy.

Strategy (% savings)	**Ada-Grad** (*Acc@1* (%), *Acc@5* (%))	**Ada-Delta** (*Acc@1* (%), *Acc@5* (%))
Baseline (0)	79.90 ± 1.25 , 94.69 ± 1.84	88.90 ± 1.14 , 99.66 ± 2.13
Pe = 5 (20)	79.50 ± 1.15 , 93.50 ± 2.64	**88.96 ± 1.15** , 99.66 ± 2.27
Pe = 10 (10)	**79.95 ± 1.30** , **94.75 ± 2.12**	**89.92 ± 1.20** , **99.68 ± 2.03**
Pr = 0.2 (20)	**79.97 ± 1.10** , **94.79 ± 1.95**	88.90 ± 1.05 , **99.68 ± 2.50**
Pr = 0.5 (50)	77.73 ± 1.20 , 93.64 ± 2.70	87.52 ± 1.30 , 99.46 ± 2.18
Pr = 0.7 (70)	75.45 ± 1.35 , 93.68 ± 1.67	87.04 ± 1.40 , 99.51 ± 2.38

Comparison with Related Works: We experimented with the recent MeZO Malladi et al. (2023) method on the SST-2 Socher et al. (2013) and RTE Dagan et al. (2005) datasets using 10k optimization steps. The results, along with the performance of our proposed strategies, are reported in Table 11.

Table 11: Performance comparison of different strategies on SST-2 and RTE datasets.

	Strategy (% savings)	**SST-2**	**RTE**
MeZO	Baseline (0)	91.28	67.57
	Pe=5 (20)	90.67	65.78
	Pe=10 (10)	**91.67**	**67.85**
	Pr=0.2 (20)	**92.07**	**67.75**
	Pr=0.5 (50)	**91.36**	67.55
	Pr=0.7 (70)	90.97	67.02

As shown in Table 11, our proposed strategies consistently outperform the baseline MeZO method in terms of accuracy on both SST-2 and RTE datasets.Notably, the sampling conditions with Pe=10 and Pr=0.2 yield improved performance compared to the baseline approach. This demonstrates the scalability and effectiveness of our method across diverse settings without compromising the performance.

5 Conclusion

We introduced a gradient sampling technique to reduce energy consumption in deep learning models, particularly for computer vision tasks such as image classification, object detection, and image segmentation. Our approach also demonstrated effectiveness in out-of-distribution scenarios, including Domain Adaptation (DA), Domain Generalization (DG), and Federated Learning (FL). We further validated its applicability in large language model (LLM) pretraining, where it achieved similar energy savings without degrading model quality. Tested across various optimizers, it proved to be robust and practical, showing that periodic and probabilistic sampling can significantly reduce energy usage without compromising performance.

References

Alexander Camuto, Matthew Willetts, Umut Simsekli, Stephen J Roberts, and Chris C Holmes. Explicit regularisation in gaussian noise injections. *Advances in Neural Information Processing Systems*, 33: 16603–16614, 2020.

Bowen Cheng, Ishan Misra, Alexander G Schwing, Alexander Kirillov, and Rohit Girdhar. Masked-attention mask transformer for universal image segmentation. In *Proceedings of the IEEE/CVF conference on computer vision and pattern recognition*, pp. 1290–1299, 2022.

Ido Dagan, Oren Glickman, and Bernardo Magnini. The pascal recognising textual entailment challenge. In *Machine Learning Challenges Workshop*, pp. 177–190. Springer, 2005.

Jia Deng, Wei Dong, Richard Socher, Li-Jia Li, Kai Li, and Li Fei-Fei. Imagenet: A large-scale hierarchical image database. In *2009 IEEE Conference on Computer Vision and Pattern Recognition*, pp. 248–255. IEEE, 2009.

Radosvet Desislavov, Fernando Martínez-Plumed, and José Hernández-Orallo. Trends in ai inference energy consumption: Beyond the performance-vs-parameter laws of deep learning. *Sustainable Computing: Informatics and Systems*, 38:100857, 2023.

Alexey Dosovitskiy, Lucas Beyer, Alexander Kolesnikov, Dirk Weissenborn, Xiaohua Zhai, Thomas Unterthiner, Mostafa Dehghani, Matthias Minderer, Georg Heigold, Sylvain Gelly, Jakob Uszkoreit, and Neil Houlsby. An image is worth 16x16 words: Transformers for image recognition at scale. In *International Conference on Learning Representations*, 2021. URL `https://openreview.net/forum?id=YicbFdNTTy`.

John C. Duchi, Elad Hazan, and Yoram Singer. Adaptive subgradient methods for online learning and stochastic optimization. *Journal of Machine Learning Research*, 12:2121–2159, 2011.

Steve K Esser, Rathinakumar Appuswamy, Paul Merolla, John V Arthur, and Dharmendra S Modha. Backpropagation for energy-efficient neuromorphic computing. *Advances in neural information processing systems*, 28, 2015.

Mark Everingham, Luc Van Gool, Christopher KI Williams, John Winn, and Andrew Zisserman. The pascal visual object classes (voc) challenge. *International Journal of Computer Vision*, 88(2):303–338, 2010. doi: 10.1007/s11263-009-0275-4. URL `http://host.robots.ox.ac.uk/pascal/VOC/`.

B. V. Gnedenko and A. N. Kolmogorov. *Limit Distributions for Sums of Independent Random Variables*. Addison-Wesley, Reading, MA, 1954.

Kaiming He, Xiangyu Zhang, Shaoqing Ren, and Jian Sun. Deep residual learning for image recognition. In *Proceedings of the IEEE conference on computer vision and pattern recognition*, pp. 770–778, 2016.

Torsten Hoefler, Dan Alistarh, Tal Ben-Nun, Nikoli Dryden, and Alexandra Peste. Sparsity in deep learning: Pruning and growth for efficient inference and training in neural networks. *The Journal of Machine Learning Research*, 22(1):10882–11005, 2021.

Tzu-Ming Harry Hsu, Hang Qi, and Matthew Brown. Measuring the effects of non-identical data distribution for federated visual classification. *arXiv preprint arXiv:1909.06335*, 2019.

Ying Jin, Ximei Wang, Mingsheng Long, and Jianmin Wang. Minimum class confusion for versatile domain adaptation. In *Computer Vision–ECCV 2020: 16th European Conference, Glasgow, UK, August 23–28, 2020, Proceedings, Part XXI 16*, pp. 464–480. Springer, 2020.

Alex Krizhevsky and Geoffrey Hinton. Learning multiple layers of features from tiny images. Technical Report TR-2009, University of Toronto, 2009. URL `https://www.cs.toronto.edu/~kriz/cifar.html`.

David Krueger, Ethan Caballero, Joern-Henrik Jacobsen, Amy Zhang, Jonathan Binas, Dinghuai Zhang, Remi Le Priol, and Aaron Courville. Out-of-distribution generalization via risk extrapolation (rex). In *ICML*, 2021.

C-C Jay Kuo and Azad M Madni. Green learning: Introduction, examples and outlook. *Journal of Visual Communication and Image Representation*, pp. 103685, 2022.

Ya Le and Xuan Yang. Tiny imagenet visual recognition challenge. `https://www.kaggle.com/c/tiny-imagenet`, 2015. Accessed: 2025-01-27.

Da Li, Yongxin Yang, Yi-Zhe Song, and Timothy M Hospedales. Deeper, broader and artier domain generalization. In *Proceedings of the IEEE international conference on computer vision*, pp. 5542–5550, 2017.

Tian Li, Anit Kumar Sahu, Ameet Talwalkar, and Virginia Smith. Federated learning: Challenges, methods, and future directions. *IEEE signal processing magazine*, 37(3):50–60, 2020a.

Tian Li, Anit Kumar Sahu, Manzil Zaheer, Maziar Sanjabi, Ameet Talwalkar, and Virginia Smith. Federated optimization in heterogeneous networks. *Proceedings of Machine learning and systems*, 2:429–450, 2020b.

Ruiyuan Lin, Zhiruo Zhou, Suya You, Raghuveer Rao, and C-C Jay Kuo. Geometrical interpretation and design of multilayer perceptrons. *IEEE Transactions on Neural Networks and Learning Systems*, 2022.

Yiheng Liu, Tianle Han, Siyuan Ma, Jiayue Zhang, Yuanyuan Yang, Jiaming Tian, Hao He, Antong Li, Mengshen He, Zhengliang Liu, et al. Summary of chatgpt/gpt-4 research and perspective towards the future of large language models. *arXiv preprint arXiv:2304.01852*, 2023.

Ze Liu, Yutong Lin, Yue Cao, Han Hu, Yixuan Wei, Zheng Zhang, Stephen Lin, and Baining Guo. Swin transformer: Hierarchical vision transformer using shifted windows. In *Proceedings of the IEEE/CVF International Conference on Computer Vision (ICCV)*, pp. 10012–10022, October 2021.

Wenyu Lv, Yian Zhao, Qinyao Chang, Kui Huang, Guanzhong Wang, and Yi Liu. Rt-detrv2: Improved baseline with bag-of-freebies for real-time detection transformer, 2024. URL `https://arxiv.org/abs/2407.17140`.

Andrew L Maas, Raymond E Daly, Peter T Pham, Dan Huang, Andrew Y Ng, and Christopher Potts. Learning word vectors for sentiment analysis. In *Proceedings of the 49th Annual Meeting of the Association for Computational Linguistics: Human Language Technologies*, pp. 142–150. Association for Computational Linguistics, 2011.

Sadhika Malladi, Tianyu Gao, Eshaan Nichani, Alex Damian, Jason D Lee, Danqi Chen, and Sanjeev Arora. Fine-tuning language models with just forward passes. *arXiv preprint arXiv:2305.17333*, 2023.

Frank J. Massey. The kolmogorov-smirnov test for goodness of fit. *Journal of the American Statistical Association*, 46:68–78, 1951. URL `https://api.semanticscholar.org/CorpusID:209842899`.

Brendan McMahan, Eider Moore, Daniel Ramage, Seth Hampson, and Blaise Aguera y Arcas. Communication-efficient learning of deep networks from decentralized data. In *Artificial intelligence and statistics*, pp. 1273–1282. PMLR, 2017.

Paul A Merolla, John V Arthur, Rodrigo Alvarez-Icaza, Andrew S Cassidy, Jun Sawada, Filipp Akopyan, Bryan L Jackson, Nabil Imam, Chen Guo, Yutaka Nakamura, et al. A million spiking-neuron integrated circuit with a scalable communication network and interface. *Science*, 345(6197):668–673, 2014.

Alec Radford, Jeffrey Wu, Rewon Child, David Luan, Dario Amodei, and Ilya Sutskever. Language models are unsupervised multitask learners. *OpenAI Blog*, 1(8):9, 2019.

Olaf Ronneberger, Philipp Fischer, and Thomas Brox. U-net: Convolutional networks for biomedical image segmentation. In *Medical image computing and computer-assisted intervention–MICCAI 2015: 18th international conference, Munich, Germany, October 5-9, 2015, proceedings, part III 18*, pp. 234–241. Springer, 2015.

David E Rumelhart, Geoffrey E Hinton, and Ronald J Williams. Learning representations by back-propagating errors. *nature*, 323(6088):533–536, 1986.

Kate Saenko, Brian Kulis, Mario Fritz, and Trevor Darrell. Adapting visual category models to new domains. In *European Conference on Computer Vision*, 2010. URL https://api.semanticscholar.org/CorpusID:7534823.

Shiori Sagawa, Pang Wei Koh, Tatsunori B. Hashimoto, and Percy Liang. Distributionally robust neural networks for group shifts: On the importance of regularization for worst-case generalization. In *ICLR*, 2020.

Umut Şimşekli, Mert Gürbüzbalaban, Thanh Huy Nguyen, Gaël Richard, and Levent Sagun. On the heavy-tailed theory of stochastic gradient descent for deep neural networks. *arXiv preprint arXiv:1912.00018*, 2019.

Richard Socher, Alex Perelygin, Jean Wu, Jason Chuang, Christopher D. Manning, Andrew Ng, and Christopher Potts. Recursive deep models for semantic compositionality over a sentiment treebank. In *Proceedings of the 2013 Conference on Empirical Methods in Natural Language Processing*, pp. 1631–1642, Seattle, Washington, USA, October 2013. Association for Computational Linguistics. URL https://www.aclweb.org/anthology/D13-1170.

Emma Strubell, Ananya Ganesh, and Andrew McCallum. Energy and policy considerations for modern deep learning research. In *Proceedings of the AAAI conference on artificial intelligence*, volume 34, pp. 13693–13696, 2020.

Robin Strudel, Ricardo Garcia, Ivan Laptev, and Cordelia Schmid. Segmenter: Transformer for semantic segmentation. In *Proceedings of the IEEE/CVF International Conference on Computer Vision (ICCV)*, pp. 7262–7272, October 2021.

Yan Sun, Li Shen, Tiansheng Huang, Liang Ding, and Dacheng Tao. Fedspeed: Larger local interval, less communication round, and higher generalization accuracy. In *The Eleventh International Conference on Learning Representations*, 2023. URL https://openreview.net/forum?id=bZjxxYURKT.

Vivienne Sze, Yu-Hsin Chen, Tien-Ju Yang, and Joel S Emer. Efficient processing of deep neural networks: A tutorial and survey. *Proceedings of the IEEE*, 105(12):2295–2329, 2017.

Ilya O Tolstikhin, Neil Houlsby, Alexander Kolesnikov, Lucas Beyer, Xiaohua Zhai, Thomas Unterthiner, Jessica Yung, Andreas Steiner, Daniel Keysers, Jakob Uszkoreit, et al. Mlp-mixer: An all-mlp architecture for vision. *Advances in neural information processing systems*, 34:24261–24272, 2021.

Chien-Yao Wang, Alexey Bochkovskiy, and Hong-Yuan Mark Liao. Yolov7: Trainable bag-of-freebies sets new state-of-the-art for real-time object detectors. In *Proceedings of the IEEE/CVF conference on computer vision and pattern recognition*, pp. 7464–7475, 2023.

Max Welling and Yee W Teh. Bayesian learning via stochastic gradient langevin dynamics. In *Proceedings of the 28th international conference on machine learning (ICML-11)*, pp. 681–688. Citeseer, 2011.

Matthew D. Zeiler. Adadelta: An adaptive learning rate method. *arXiv preprint arXiv:1212.5701*, 2012.

Yuchen Zhang, Tianle Liu, Mingsheng Long, and Michael Jordan. Bridging theory and algorithm for domain adaptation. In *ICML*, 2019.

Bolei Zhou, Hang Zhao, Xavier Puig, Sanja Fidler, Adela Barriuso, and Antonio Torralba. Scene parsing through ade20k dataset. *Proceedings of the IEEE Conference on Computer Vision and Pattern Recognition (CVPR)*, pp. 633–641, 2017. URL http://groups.csail.mit.edu/vision/datasets/ADE20K/.

A Theorem 3.1 Proof:

Suppose $\hat{\boldsymbol{\delta}}^{(k)} \sim \text{GGD}((\boldsymbol{\theta}^{(k)} - \boldsymbol{\theta}^{(k-1)}); \mu^{(k)}, \sigma^{(k)}, \beta^{(k)})$, where GGD denotes the Generalized Gaussian Distribution. Then, the parameter update at the $(k{+}1)$-th iteration, when sampling via SGD, is given by:

$$\boldsymbol{\theta}^{(k+1)} = \begin{cases} \boldsymbol{\theta}^{(k)} + \hat{\boldsymbol{\delta}}^{(k)} & \text{with probability } \rho \\ \boldsymbol{\theta}^{(k)} - \eta \nabla \mathcal{L}(\boldsymbol{\theta}^{(k)}) & \text{with probability } (1-\rho) \end{cases}$$

The expected value of the loss at the next iteration, $\mathbb{E}[\mathcal{L}(\boldsymbol{\theta}^{(k+1)})]$, can be written as:

$$\mathbb{E}[\mathcal{L}(\boldsymbol{\theta}^{(k+1)})] = \rho \left[\underbrace{\mathbb{E}[\mathcal{L}(\boldsymbol{\theta}^{(k+1)})|\text{GGD}]}_{\text{Lemma A.1}} \right] + (1-\rho) \left[\underbrace{\mathbb{E}[\mathcal{L}(\boldsymbol{\theta}^{(k+1)})|\text{SGD}]}_{\text{Lemma A.2}} \right] \tag{13}$$

Lemma A.1. *Assume that the function $\mathcal{L}(\boldsymbol{\theta}^{(k)})$ is L'-Lipschitz continuous, with $\mathbb{E}[\hat{\boldsymbol{\delta}}^{(k)}] = \mu^{(k)} = 0$ and $\mathbb{E}[||\hat{\boldsymbol{\delta}}^{(k)}||^2] \leq {\sigma^{(k)}}^2$ (bounded). Then,*

$$\mathbb{E}[\mathcal{L}(\boldsymbol{\theta}^{(k+1)})] \leq \mathbb{E}[\mathcal{L}(\boldsymbol{\theta}^{(k)})] + \frac{L'{\sigma^{(k)}}^2}{2}.$$

Proof. Since $\mathcal{L}(.)$ is L'-Lipschitz continuous, with $\mathbb{E}[\hat{\boldsymbol{\delta}}^{(k)}] = \mu^{(k)} = 0, \quad \mathbb{E}[||\hat{\boldsymbol{\delta}}^{(k)}||^2] \leq {\sigma^{(k)}}^2$, we have:

$$\begin{aligned} \mathcal{L}(\boldsymbol{\theta}^{(k+1)}) &\leq \mathcal{L}(\boldsymbol{\theta}^{(k)}) + \nabla \mathcal{L}(\boldsymbol{\theta}^{(k)})^\top \hat{\boldsymbol{\delta}}^{(k)} + \frac{L'}{2}||\hat{\boldsymbol{\delta}}^{(k)}||^2 \\ \mathbb{E}[\mathcal{L}(\boldsymbol{\theta}^{(k+1)})] &\leq \mathbb{E}[\mathcal{L}(\boldsymbol{\theta}^{(k)})] + \frac{L'{\sigma^{(k)}}^2}{2}. \end{aligned} \tag{14}$$

□

Lemma A.2. *Assume that the function $\mathcal{L}(\boldsymbol{\theta}^{(k)})$ is both L'-Lipschitz continuous and μ'-strongly convex. Then $\boldsymbol{\theta}^{(k+1)}$ follows the SGD update rule:*

$$\mathbb{E}[\mathcal{L}(\boldsymbol{\theta}^{(k+1)})] \leq \mathbb{E}[\mathcal{L}(\boldsymbol{\theta}^{(*)})] + (1 - 2\mu'\eta)\Delta_k,$$

where $\Delta_k = \mathbb{E}[\mathcal{L}(\boldsymbol{\theta}^{(k)}) - \mathcal{L}(\boldsymbol{\theta}^{(*)})]$ and $\boldsymbol{\theta}^{(*)}$ is the optimal parameter.

Proof. Since $\mathcal{L}(.)$ is L'-Lipschitz continuous, we have:

$$\begin{aligned} \mathcal{L}(\boldsymbol{\theta}^{(k+1)}) &\leq \mathcal{L}(\boldsymbol{\theta}^{(k)}) + \nabla \mathcal{L}(\boldsymbol{\theta}^{(k)})^\top (-\eta \nabla \mathcal{L}(\boldsymbol{\theta}^{(k)})) + \frac{L'}{2}|| - \eta \nabla \mathcal{L}(\boldsymbol{\theta}^{(k)})||^2 \\ &\leq \mathcal{L}(\boldsymbol{\theta}^{(k)}) - \left(\eta - \frac{L'}{2}\eta^2\right) ||\nabla \mathcal{L}(\boldsymbol{\theta}^{(k)})||^2 \end{aligned} \tag{15}$$

Since $\mathcal{L}(.)$ is μ'-strongly convex, we have the inequality:

$$||\nabla \mathcal{L}(\boldsymbol{\theta}^{(k)})||^2 \geq 2\mu'(\mathcal{L}(\boldsymbol{\theta}^{(k)}) - \mathcal{L}(\boldsymbol{\theta}^{(*)})) \tag{16}$$

Substituting equation 16 into equation 15, we get:

$$\begin{aligned} \mathcal{L}(\boldsymbol{\theta}^{(k+1)}) &\leq \mathcal{L}(\boldsymbol{\theta}^{(k)}) - 2\mu' \left(\eta - \frac{L'}{2}\eta^2\right) (\mathcal{L}(\boldsymbol{\theta}^{(k)}) - \mathcal{L}(\boldsymbol{\theta}^{(*)})) \\ \mathcal{L}(\boldsymbol{\theta}^{(k+1)}) &\leq \mathcal{L}(\boldsymbol{\theta}^{(*)}) + (1 - 2\mu'\eta + L'\mu'\eta^2)(\mathcal{L}(\boldsymbol{\theta}^{(k)}) - \mathcal{L}(\boldsymbol{\theta}^{(*)})) \end{aligned}$$

Taking $\mathbb{E}[\cdot]$ on both sides

$$\mathbb{E}[\mathcal{L}(\boldsymbol{\theta}^{(k+1)})] \leq \mathbb{E}[\mathcal{L}(\boldsymbol{\theta}^{(*)})] + (1 - 2\mu'\eta + L'\mu'\eta^2)\Delta_k \quad \left(\Delta_k = \mathbb{E}[\mathcal{L}(\boldsymbol{\theta}^{(k)}) - \mathcal{L}(\boldsymbol{\theta}^{(*)})]\right) \tag{17}$$

□

Combining equation 14 and equation 17, we can rewrite equation equation 13 as:

$$\mathbb{E}[\mathcal{L}(\boldsymbol{\theta}^{(k+1)})] \leq \rho \left[\mathbb{E}[\mathcal{L}(\boldsymbol{\theta}^{(k)})] + \frac{L'\sigma^{(k)^2}}{2} \right] + (1-\rho) \left[\mathbb{E}[\mathcal{L}(\boldsymbol{\theta}^{(*)})] + (1 - 2\mu'\eta + L'\mu'\eta^2)\Delta_k \right].$$

Rearranging this, we obtain the following recurrence relation for the loss difference:

$$\begin{aligned}
\mathbb{E}[\mathcal{L}(\boldsymbol{\theta}^{(k+1)})] &\leq \rho \left(\underbrace{\mathbb{E}[\mathcal{L}(\boldsymbol{\theta}^{(k)}) - \mathcal{L}(\boldsymbol{\theta}^{(*)})]}_{\Delta_k} \right) + \frac{\rho L'\sigma^{(k)^2}}{2} + \mathbb{E}[\mathcal{L}(\boldsymbol{\theta}^{(*)})] + (1-\rho)(1 - 2\mu'\eta + L'\mu'\eta^2)\Delta_k \\
\Delta_{k+1} &\leq \rho\Delta_k + (1-\rho)(1 - 2\mu'\eta + L'\mu'\eta^2)\Delta_k + \frac{\rho L'\sigma^{(k)^2}}{2} \\
\Delta_{k+1} &\leq \left(\underbrace{(1 - (1-\rho)(2\mu'\eta - L'\mu'\eta^2)}_{\gamma} \right) \Delta_k + \frac{\rho L'\sigma^{(k)^2}}{2} \qquad (18)
\end{aligned}$$

Now, we analyze the recurrence relation for the loss difference:

$$\Delta_k = \mathbb{E}[\mathcal{L}(\boldsymbol{\theta}^{(k)}) - \mathcal{L}(\boldsymbol{\theta}^{(*)})].$$

At steady state ($k \to \infty$), we assume that $\Delta_{k+1} = \Delta_k = \Delta_*$. Substituting this into the recurrence relation, we get:

$$\Delta_* = \gamma\Delta_* + \frac{\rho L'\sigma^{(k)^2}}{2}.$$

Rearranging the terms:

$$\Delta_*(1-\gamma) = \frac{\rho L'\sigma^{(k)^2}}{2},$$

which simplifies to:

$$\Delta_* = \frac{\rho L'\sigma^{(k)^2}}{2(1-\gamma)}.$$

Substituting $\gamma = 1 - (1-\rho)(2\mu'\eta - L'\mu'\eta^2)$, we get:

$$\Delta_* = \frac{\rho L'\sigma^{(k)^2}}{2(1-\rho)(2\mu'\eta - L'\mu'\eta^2)}.$$

Next, we consider the transient behavior. The recurrence relation for the loss difference is:

$$\Delta_{k+1} = \gamma\Delta_k + \frac{\rho L'\sigma^{(k)^2}}{2}.$$

The general solution to this recurrence is:

$$\Delta_k = (\Delta_0 - \Delta_*)\gamma^k + \Delta_*,$$

where $\Delta_0 = \mathbb{E}[\mathcal{L}(\boldsymbol{\theta}^{(0)}) - \mathcal{L}(\boldsymbol{\theta}^{(*)})]$ is the initial loss difference. The convergence rate of the recurrence is determined by the term $(\Delta_0 - \Delta_*)\gamma^k$, which decays exponentially as k increases. Since $0 < \gamma < 1$, the rate of decay is controlled by $\gamma = 1 - (1-\rho)(2\mu'\eta - L'\mu'\eta^2)$. For convergence to occur, we require $0 < \gamma < 1$.

The steady-state value Δ_* is proportional to:

$$\Delta_* \propto \frac{\rho L' {\sigma^{(k)}}^2}{(1-\rho)(2\mu'\eta - L'\mu'\eta^2)}.$$

This implies that increasing μ' (the strong convexity constant) or η (the learning rate) reduces the steady-state error Δ_*. The steady-state error also depends on the probability ρ, which governs the sampling process. As ρ increases, the term $\gamma = 1 - (1-\rho)(2\mu'\eta - L'\mu'\eta^2)$ approaches 1, slowing down convergence and increasing the steady-state error. Specifically, when $\rho = 0$, the convergence occurs at the fastest rate, with $\gamma = 1 - (1-\rho)(2\mu'\eta - L'\mu'\eta^2)$, and the convergence speed primarily depends on η and μ'. In this case, the steady-state error is smaller, and convergence is faster.

However, as ρ approaches 1, the convergence slows due to the diminished effect of the decay factor γ. The optimal value of ρ balances the trade-off between convergence speed and steady-state error: smaller values of ρ lead to faster convergence and smaller steady-state error, while larger values lead to slower convergence and higher steady-state error. Furthermore, the steady-state error Δ_* is influenced by the Lipschitz constant L' of the loss function. A larger L' increases the steady-state error, indicating that the loss function is more sensitive to changes in parameters. To reduce steady-state error, it is desirable to have a smaller L'.

To ensure stability, the learning rate η must satisfy:

$$0 < \eta < \min\left\{\tfrac{2}{L'}, \tfrac{1}{2\mu'(1-\rho)}\right\}, \quad \text{(Lemma } A.3\text{)}$$

which guarantees that $\gamma < 1$ and ensures geometric convergence. If η exceeds this threshold, updates may overshoot, leading to instability and preventing convergence.

In conclusion, the recurrence relation is:

$$\Delta_{k+1} = \gamma\Delta_k + \frac{\rho L' {\sigma^{(k)}}^2}{2},$$

with the steady-state value:

$$\Delta_* = \frac{\rho L' {\sigma^{(k)}}^2}{2(1-\rho)(2\mu'\eta - L'\mu'\eta^2)}.$$

and the general solution:

$$\Delta_k = (\Delta_0 - \Delta_*)\gamma^k + \Delta_*.$$

The convergence rate is geometric with rate:

$$\gamma = 1 - (1-\rho)(2\mu'\eta - L'\mu'\eta^2).$$

The algorithm converges with complexity:

$$\mathcal{O}\left(\gamma^k\right) \Rightarrow \mathcal{O}\left(\left(1 - (1-\rho)(2\mu'\eta - L'\mu'\eta^2)\right)^k\right).$$

Lemma A.3. *Assume that the function $\mathcal{L}(\boldsymbol{\theta}^{(k)})$ is both L'-Lipschitz continuous and μ'-strongly convex. Let ρ be the sampling probability with $\gamma = 1 - (1-\rho)(2\mu'\eta - L'\mu'\eta^2)$ being the decaying rate. From this point onwards, to ensure convergence, the learning rate η must satisfy*

$$0 < \eta < \min\left\{\tfrac{2}{L'}, \tfrac{1}{2\mu'(1-\rho)}\right\}.$$

Proof. To ensure convergence, the following expression $\gamma = 1-(1-\rho)(2\mu'\eta - L'\mu'\eta^2)$ must strictly lie between 0 and 1, we require

$$0 < \gamma < 1.$$

This leads to two inequalities.

1. **Upper Bound ($\gamma < 1$)**

$$\begin{aligned} \gamma &< 1, \text{or} \\ 1-(1-\rho)(2\mu'\eta - L'\mu'\eta^2) &< 1, \text{or equivalently} \\ -(1-\rho)(2\mu'\eta - L'\mu'\eta^2) &< 0. \end{aligned}$$

   Since $(1-\rho) > 0$ (as $0 \le \rho < 1$),

$$\begin{aligned} 2\mu'\eta - L'\mu'\eta^2 &> 0, \text{or} \\ \mu'\eta(2 - L'\eta) &> 0. \end{aligned}$$

   Since $\mu' > 0$ and $\eta > 0$, we require:

$$2 - L'\eta > 0 \quad \Rightarrow \quad \eta < \frac{2}{L'}.$$

   Thus, the upper bound is

$$\eta < \frac{2}{L'}.$$

—

2. **Lower Bound ($\gamma > 0$)**

$$\begin{aligned} \gamma &> 0, \text{or} \\ 1-(1-\rho)(2\mu'\eta - L'\mu'\eta^2) &> 0, \text{or equivalently} \\ (1-\rho)(2\mu'\eta - L'\mu'\eta^2) &< 1. \end{aligned}$$

   As before, since $(1-\rho) > 0$,

$$2\mu'\eta - L'\mu'\eta^2 < \frac{1}{1-\rho}.$$

   Let

$$f(\eta) = 2\mu'\eta - L'\mu'\eta^2.$$

   This is a concave quadratic with maximum at

$$\eta^* = \frac{1}{L'}.$$

   The maximum value is

$$f(\eta^*) = \frac{\mu'}{L'}.$$

Hence, we require

$$\frac{\mu'}{L'} < \frac{1}{1-\rho},$$

which gives a condition on the parameters:

$$\mu' < \frac{L'}{1-\rho}.$$

If this holds, then for all $0 < \eta < \frac{2}{L'}$, the inequality is satisfied.

—

3. **Case when $\frac{\mu'}{L'} \geq \frac{1}{1-\rho}$** If instead $\frac{\mu'}{L'} \geq \frac{1}{1-\rho}$, then we must solve explicitly:

$$2\mu'\eta - L'\mu'\eta^2 < \frac{1}{1-\rho}.$$

Equivalently:

$$L'\mu'\eta^2 - 2\mu'\eta + \frac{1}{1-\rho} > 0.$$

The roots of

$$L'\mu'\eta^2 - 2\mu'\eta + \frac{1}{1-\rho} = 0$$

are

$$\eta = \frac{1 \pm \sqrt{1 - \frac{L'}{\mu'(1-\rho)}}}{L'}.$$

For real roots, we need

$$\mu'(1-\rho) \geq L'.$$

In this case, since the quadratic opens upward, the inequality holds for

$$\eta < \frac{1 - \sqrt{1 - \frac{L'}{\mu'(1-\rho)}}}{L'} \quad \text{or} \quad \eta > \frac{1 + \sqrt{1 - \frac{L'}{\mu'(1-\rho)}}}{L'}.$$

But combined with $\eta < \frac{2}{L'}$, the lower branch is the relevant range.

—

4. **Simplified Practical Bound** In practice, to avoid complexity, we ensure

$$\frac{\mu'}{L'} < \frac{1}{1-\rho},$$

which is usually satisfied if ρ is not too close to 1 and μ' is not too large relative to L'. Thus, a safe step-size bound is

$$0 < \eta < \min\left\{\frac{2}{L'}, \frac{1}{2\mu'(1-\rho)}\right\}.$$

This ensures both conditions are met:

- $\eta < \frac{2}{L'}$ from $\gamma < 1$,
- $\eta < \frac{1}{2\mu'(1-\rho)}$ from $\gamma > 0$

5. **Final Result:**

$$\boxed{0 < \eta < \min\left\{\frac{2}{L'}, \frac{1}{2\mu'(1-\rho)}\right\}}$$

□

B Technical details:

Table 12: Technical specifications across various tasks.

Task	Models	Datasets	Metrics	Backbone / Component
Image Classification	ResNet-50 (He et al., 2016) Swin-T (Liu et al., 2021) MLP-Mixer (Tolstikhin et al., 2021)	CIFAR-10 (Krizhevsky & Hinton, 2009) CIFAR-100 (Krizhevsky & Hinton, 2009) Tiny ImageNet (Le & Yang, 2015) ImageNet (Deng et al., 2009)	*Acc @1* *Acc @5*	—
Object Detection	YOLOv7 (Wang et al., 2023) RT-DETRv2 (Lv et al., 2024)	Pascal VOC 2012 (Everingham et al., 2010)	*mAP @0.5* *mAP @0.5:0.95*	—
Image Segmentation	U-Net (Ronneberger et al., 2015) Segmenter-Tiny (Strudel et al., 2021)	ADE20K (Zhou et al., 2017)	*SS-IoU* *MS-IoU*	U-Net: ResNet-34 (He et al., 2016) Segmenter: ViT (Dosovitskiy et al., 2021) encoder + MaskFormer (Cheng et al., 2022) decoder
Domain Adaptation (DA)	MDD (Zhang et al., 2019) MCC (Jin et al., 2020)	Office-31 (Saenko et al., 2010)	*Acc @1*	ResNet-50 (He et al., 2016)
Domain Generalization (DG)	VREx (Krueger et al., 2021) GroupDRO (Sagawa et al., 2020)	PACS (Li et al., 2017)	*Acc @1*	ResNet-50 (He et al., 2016)
Federated Learning (FL)	`FedAvg` (McMahan et al., 2017) `FedProx` (Li et al., 2020b) `FedSpeed` (Sun et al., 2023)	CIFAR-10 (Krizhevsky & Hinton, 2009)	*Acc @1*	ResNet-50 (He et al., 2016)
LLM Pre-training	GPT-2 (Radford et al., 2019)	IMDB (Maas et al., 2011)	Accuracy Precision Recall F1-Score	—

C Implementation Details:

Image Classification:

Image Classification Task	
Repository:	https://github.com/microsoft/Swin-Transformer
Implementations:	Integrated with various models and datasets
Total Epochs:	200 (Default: 300)
Warmup Epochs:	1 (Default: 20)
Trials:	3
AdaDelta Optimizer	
Learning Rate (η):	0.1
Warmup Epochs:	20
AdaGrad Optimizer	
Learning Rate (η):	Default Value
Warmup Epochs:	20

Table 13: Hyperparameters for the Image Classification Task

Object Detection:

Object Detection Task	
Repositories:	**YOLOv7:** https://github.com/WongKinYiu/yolov7 **RT-DETRv2:** https://github.com/lyuwenyu/RT-DETR
Epochs:	YOLOv7: 100, RT-DETRv2: 72 (Default)

Table 14: Hyperparameters for the Object Detection Task

Image Segmentation:

Image Segmentation Task	
Repository:	https://github.com/rstrudel/segmenter
Models:	Segmenter (Strudel et al., 2021), U-Net (Ronneberger et al., 2015)
Training Epochs:	20 (Default)

Table 15: Hyperparameters for the Image Segmentation Task

Domain Adaptation (DA) and Domain Generalization (DG):

Domain Adaptation (DA) and Domain Generalization (DG)	
Repository:	https://github.com/thuml/Transfer-Learning-Library
Methods:	MDD (Zhang et al., 2019), MCC (Jin et al., 2020), Vrex (Krueger et al., 2021), GroupDRO (Sagawa et al., 2020)
Training Schedule:	200 iterations per epoch, 20 epochs

Table 16: Hyperparameters for Domain Adaptation and Domain Generalization Experiments

Federated Learning:

Federated Learning (FL)	
Repository:	https://github.com/woodenchild95/FL-Simulator
Methods:	FedAvg (McMahan et al., 2017), FedProx (Li et al., 2020b), FedSpeed (Sun et al., 2023)

Table 17: Hyperparameters for Federated Learning (FL) Experiments

For all our experiments, we kept other parameters unchanged.

D Actual vs Effective BackPropagations:

Table 18 compares the number of **backpropagation operations** under different **sampling strategies**, highlighting the **efficiency gains** achieved through sampling. For example, with **Pe = 5** over **200 epochs**, the training involves **167 backpropagations** and **33 sampled iterations**, whereas the baseline **without sampling** performs **167 backpropagations** and **0 sampled steps**. Performance is reported across **CIFAR-10**, **CIFAR-100**, and **Tiny ImageNet** datasets as **(with sampling, without sampling)**.

E Experiments with different Activation functions:

As shown in Table 19, our proposed sampling strategy demonstrates consistent effectiveness across various activation functions. Despite reducing the number of training epochs, the strategy maintains competitive accuracy levels, indicating its robustness and generalizability in different architectural settings.

Table 18: Comparison of **backpropagation operations** with and without **sampling strategies**, demonstrating **efficiency gains** across CIFAR-10, CIFAR-100, and Tiny ImageNet over 200 epochs. Reported metrics follow the format **(with sampling, without sampling)**, and the **higher value in each tuple is bolded**.

Model	# Backprops	CIFAR-10		CIFAR-100		TINY	
		Acc @1(↑)	*Acc* @5(↑)	*Acc* @1(↑)	*Acc* @5(↑)	*Acc* @1(↑)	*Acc* @5(↑)
ResNet-50	Pe=5(167)	(**90.69**,88.53)	(**99.67**,97.21)	(**68.62**,66.54)	(**90.53**,88.83)	(**65.40**,63.24)	(**85.60**,83.73)
	Pe=10(183)	(**91.29**,89.02)	(**99.78**,97.82)	(**68.90**,66.93)	(**90.98**,89.31)	(**66.00**,63.85)	(**86.00**,84.23)
	Pr=0.2(176)	(**90.87**,88.82)	(**99.66**,97.53)	(**69.36**,67.25)	(**90.87**,89.05)	(**65.86**,63.92)	(**86.24**,84.56)
	Pr=0.5(135)	(**90.16**,88.27)	(**99.68**,97.65)	(**66.86**,64.58)	(**90.06**,88.45)	(**63.48**,61.23)	(**84.84**,83.07)
	Pr=0.7(119)	(**89.32**,87.04)	(**99.57**,97.02)	(**64.97**,63.26)	(**89.25**,87.53)	(**62.10**,60.08)	(**84.08**,82.34)
Swin-T	Pe=5(167)	(**85.17**,83.52)	(**99.30**,96.54)	(**64.66**,62.73)	(**88.77**,86.81)	(**63.08**,61.04)	(**84.96**,83.14)
	Pe=10(183)	(**86.36**,84.85)	(**99.41**,96.91)	(**65.36**,63.65)	(**89.11**,87.34)	(**64.52**,62.57)	(**85.22**,83.54)
	Pr=0.2(176)	(**85.99**,84.53)	(**99.35**,96.83)	(**65.72**,63.82)	(**88.97**,87.02)	(**63.60**,61.85)	(**85.04**,83.35)
	Pr=0.5(135)	(**83.71**,82.04)	(**99.14**,96.23)	(**62.06**,60.25)	(**87.53**,85.54)	(**61.50**,59.58)	(**83.60**,81.83)
	Pr=0.7(119)	(**81.67**,80.07)	(**98.99**,96.04)	(**59.67**,57.84)	(**86.11**,84.02)	(**59.44**,57.23)	(**82.22**,80.15)
MLP-Mixer	Pe=5(167)	(**81.47**,79.53)	(**99.00**,95.82)	(**55.88**,54.03)	(**82.75**,81.04)	(**53.60**,52.04)	(**77.48**,76.07)
	Pe=10(183)	(**81.79**,79.83)	(**99.02**,95.91)	(**57.27**,55.57)	(**83.84**,81.85)	(**55.00**,53.35)	(**78.76**,77.13)
	Pr=0.2(176)	(**81.18**,79.34)	(**98.98**,95.75)	(**57.24**,55.38)	(**83.58**,81.64)	(**54.02**,52.53)	(**78.30**,76.52)
	Pr=0.5(135)	(**80.27**,78.58)	(**98.83**,95.54)	(**54.06**,52.27)	(**81.71**,80.02)	(**51.70**,50.04)	(**76.38**,75.03)
	Pr=0.7(119)	(**78.67**,77.04)	(**98.70**,95.24)	(**51.59**,50.03)	(**80.08**,78.34)	(**49.24**,47.83)	(**75.06**,73.54)

Table 19: Acc@1 and Acc@5 (%) with different sampling strategies across activation functions (*ReLU*, *Sigmoid*, *Tanh*). Values are bolded if they exceed the corresponding baseline values.

Strategy	**Acc@1 (%)**			**Acc@5 (%)**		
	ReLU	*Sigmoid*	*Tanh*	*ReLU*	*Sigmoid*	*Tanh*
Baseline	98.06	95.68	97.90	99.95	99.82	99.96
Pe = 5	98.03	95.17	**97.97**	**99.96**	**99.88**	**99.97**
Pe = 10	**98.07**	**95.91**	**97.96**	**99.96**	**99.89**	**99.98**
Pr = 0.2	**98.15**	**95.92**	**97.98**	**99.96**	**99.87**	**99.98**
Pr = 0.5	97.89	94.87	97.62	**99.96**	**99.85**	**99.98**
Pr = 0.7	97.86	94.37	97.48	99.95	99.74	99.90

F Random Noise vs GGD

we experimented by replacing GGD with some random noise below $\mathcal{N}(0, 0.01)$ and reported in the Table 20 in the revised manuscript. The table below clearly shows that our method maintains superior performance, even when replaced with random noise.

Table 20: CIFAR-100 accuracies (Top-1, Top-5) and Random Noise performance for different strategies on ResNet-50 and Swin-T. Baseline is highlighted, best Top-1 and Top-5 per model are bolded. Random Noise reports lower performance than standard evaluation.

Models	Strategy (#effective backprops)	GGD (Top-1, Top-5)	$\mathcal{N}$(0,0.01)(Top-1, Top-5)
ResNet-50	**Baseline (200)**	(69.96, 91.64)	-
	Pe = 5 (167)	(68.02, 90.39)	(65.10, 88.50)
	Pe = 10 (183)	(**69.98**, **91.86**)	(67.20, 90.30)
	Pr = 0.2 (176)	(68.42, 91.77)	(66.50, 90.00)
	Pr = 0.5 (135)	(65.90, 89.71)	(63.80, 87.90)
	Pr = 0.7 (119)	(64.21, 89.05)	(61.50, 86.20)
Swin-T	**Baseline (200)**	(64.53, 88.58)	-
	Pe = 5 (167)	(61.95, 87.05)	(59.10, 84.50)
	Pe = 10 (183)	(**64.86**, **88.66**)	(62.80, 86.90)
	Pr = 0.2 (176)	(64.58, 88.59)	(62.00, 86.30)
	Pr = 0.5 (135)	(57.99, 84.96)	(55.50, 82.10)
	Pr = 0.7 (119)	(55.41, 83.25)	(53.00, 80.50)

G Analysing the error margins:

We analyze the error margins by applying our sampling strategies on **Tiny-ImageNet** across 15 independent trials, as reported in Table 21. The results reveal that the observed error margins remain consistently tight, demonstrating the stability of our approach. More importantly, even when several epochs are skipped due to the sampling strategies, the performance does not degrade compared to the baseline for both **ResNet-50** and **Swin Transformer**. This consistency across multiple trials highlights that our method not only reduces the number of effective backpropagation operations but also achieves this efficiency **without compromising accuracy** or reliability.

Table 21: Swin Transformer on Tiny-ImageNet over 15 trials, reporting Top-1 and Top-5 accuracies. Narrow confidence intervals (0.10–0.25) support reliable conclusions.

Strategy	Accuracy (Top-1, Top-5)
Baseline	(63.12 $\pm$ 0.18, 85.01 $\pm$ 0.22)
Pe=5	(62.58 $\pm$ 0.21, 83.65 $\pm$ 0.17)
Pe=10	**(63.42 $\pm$ 0.14, 85.21 $\pm$ 0.20)**
Pr=0.2	**(63.31 $\pm$ 0.23, 85.19 $\pm$ 0.19)**
Pr=0.5	(59.34 $\pm$ 0.20, 81.95 $\pm$ 0.24)
Pr=0.7	(59.91 $\pm$ 0.16, 81.26 $\pm$ 0.21)
DP=5	(61.89 $\pm$ 0.22, 84.05 $\pm$ 0.18)
DP=10	**(63.15 $\pm$ 0.13, 85.25 $\pm$ 0.16)**
DR=0.2	**(63.15 $\pm$ 0.20, 85.23 $\pm$ 0.15)**
DR=0.5	(61.42 $\pm$ 0.17, 84.06 $\pm$ 0.22)
DR=0.7	(60.83 $\pm$ 0.19, 83.61 $\pm$ 0.24)